

PAPER • OPEN ACCESS

## Analysis of the Francis turbine upper-part-load pulsation Part II – Mechanism of self-excitation

To cite this article: P K Dörfler 2019 *IOP Conf. Ser.: Earth Environ. Sci.* **240** 052023

View the [article online](#) for updates and enhancements.

# Analysis of the Francis turbine upper-part-load pulsation Part II – Mechanism of self-excitation

**P K Dörfler**

Consulting engineer, Hydro adviser LLC, Zurich (Switzerland)

E-mail: [contact@hydroadviser.ch](mailto:contact@hydroadviser.ch)

**Abstract.** When a Francis turbine operates at partial load or very high load, the swirling flow in the draft tube may cause objectionable oscillations of pressure and power. The cavitating core of the vortex plays an important role in these pulsations. The present paper deals with a class of self-excited oscillations of the entire water column in the power plant; self-excitation means that at least one eigenvalue of the hydraulic system becomes unstable. A one-dimensional (1D) model in frequency domain explains how the normal damping is eliminated. Oscillation power is provided in regions whose flow gain in streamwise direction has a component in phase with pressure. The model contains a module for the dynamic transmission behavior of the cavitating vortex; it represents the response of the cavity size to variations of the local pressure and swirl. The sensitivity to pressure changes (the ‘cavitation compliance’) controls the natural frequencies but cannot cause instability whereas the response to swirl changes (‘mass flow gain’) may supply net oscillation energy and thus cause instability. Both influences act all along the cavitating part of the vortex; it is crucial that the variation of runner exit swirl can propagate along the vortex only with the axial velocity of the fluid. The oscillation energy balance depends on the wavelength of swirl variation, i.e. the combination of axial velocity and oscillation frequency. All instabilities of this class are ‘breathing’ pulsations, synchronous within one cross section. In the simplest case with the lowest natural frequency the pressure variation is roughly synchronous in the whole draft tube; for this mode (full-load surge) a lumped-parameter model may be adequate. By contrast, the upper-part-load pulsation occurs in a more complex eigenmode; a distributed-parameter model version is required to represent the essential features. The draft tube pressure oscillation has two quarter waves and a pressure node within the cavitation zone. The pressure at both ends of the draft tube cavitation zone has roughly opposite phase. Difficulties to transpose the stability between reduced-scale model and prototype are explained using the 1D model, as well as some influence of the runner hub shape and of the upstream conduit. Damping at the runner explains why the pulsation is limited to low-head turbines.

## 1. Introduction

Since its discovery in the early 1990s [2][3], the upper part load pulsation of the Francis turbines has been described in several publications, sometimes in considerable detail [4]. It has a well-known set of properties by which it qualifies as a self-excited breathing pulsation of the vortex cavity in the draft tube; this is described in Part I of this analysis [9]. The present paper analyses the common mechanism supplying the oscillation energy for this pulsation and other self-excited oscillations like the full-load surge. A one-dimensional model of the cavitating draft tube flow embedded in a linear time-invariant hydraulic system model is examined in frequency domain using a transfer matrix method.





connection of  $n_s$  elements (structured according to Figure 1) and embedded as reach 3 in a system according to Figure 2, with constant pressure at either end. Two pipe elements with uniform properties are representing the penstock (1) and the end diffuser (4) of the draft tube.

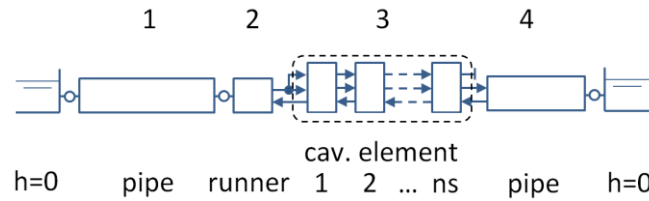


**Figure 2.** System configuration for examples 1 and 2

Figure 3 indicates in a qualitative manner the influence of the turbine discharge  $Q$  on the cavitation volume  $V_C$  in a Francis draft tube. It is the derivative  $\partial V_C / \partial Q (= -\chi)$  of this curve that can promote instability; therefore the shaded regions with steep slope are candidates for self-excited pulsations.

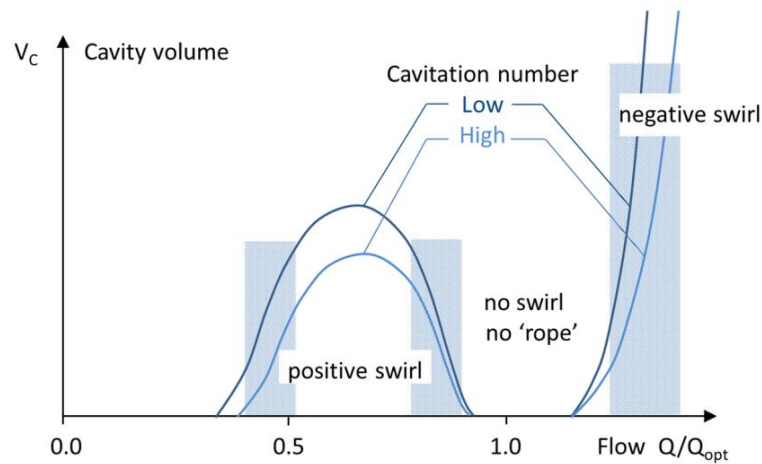


**Figure 3.** Cavitation volume vs. turbine discharge

### 3. Sample calculations

#### 3.1. Example 1: Lowest eigenmode

For easier understanding of the destabilizing effect, a simple example is described first. The data for this case (a case of full-load instability) corresponds to field test results discussed in chapters 1.5 and 8.2 of ref. [1], and is given in Table 1.

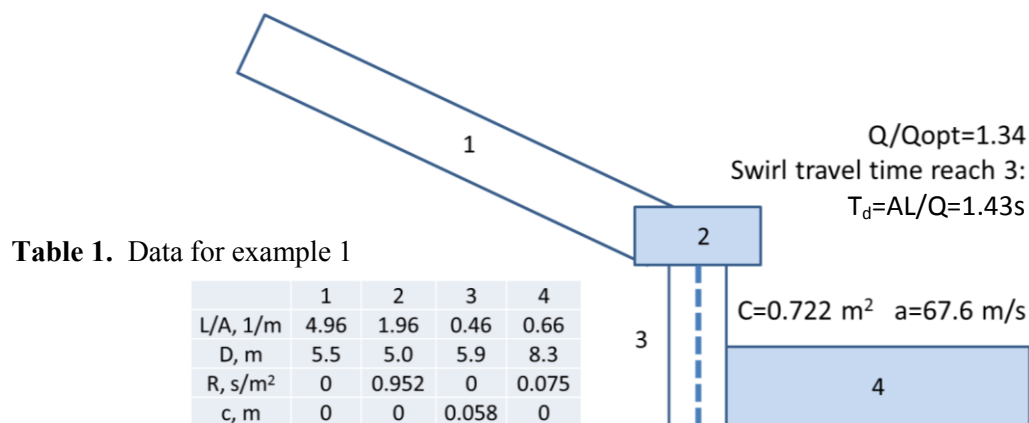


**Table 1.** Data for example 1

	1	2	3	4
L/A, 1/m	4.96	1.96	0.46	0.66
D, m	5.5	5.0	5.9	8.3
R, s/m <sup>2</sup>	0	0.952	0	0.075
c, m	0	0	0.058	0

**Figure 4.** System configuration for example 1

The axial variation of draft tube diameter, compliance and mass flow gain is neglected. Figure 4 shows the structure of the hydraulic system. In this case (full-load instability) there has to be high negative mass flow gain. In absence of the swirl transport delay  $T_d$ , no instability would occur in this case, or in any other Francis turbine with a fairly short penstock; hence the actual instability at the prototype can only be understood considering the dead time  $T_d$ .

The cavitation compliance for this case can easily be determined because the natural frequency of the pulsation has been measured. The other two parameters ( $\chi$  and  $T_d$ ) have been systematically varied in the frequency-domain model; the lowest oscillating eigenvalue of this system was computed for all combinations. The resulting distribution of eigenvalues is the stability diagram in Figure 5 (a). The main results are:

- A weak relationship between the cavitation parameters ( $\chi$  and  $T_d$ ) and the lowest eigenvalue  $s = \omega_e \cdot (\pm j - \zeta)$ , described by the natural frequency  $f = \omega_e/2\pi$  and the damping ratio  $\zeta$  (zeta).
- The decisive influence of the swirl transport time  $T_d = td(L_C)$  on stability; without the delay, this system with negative mass flow gain would always remain stable.

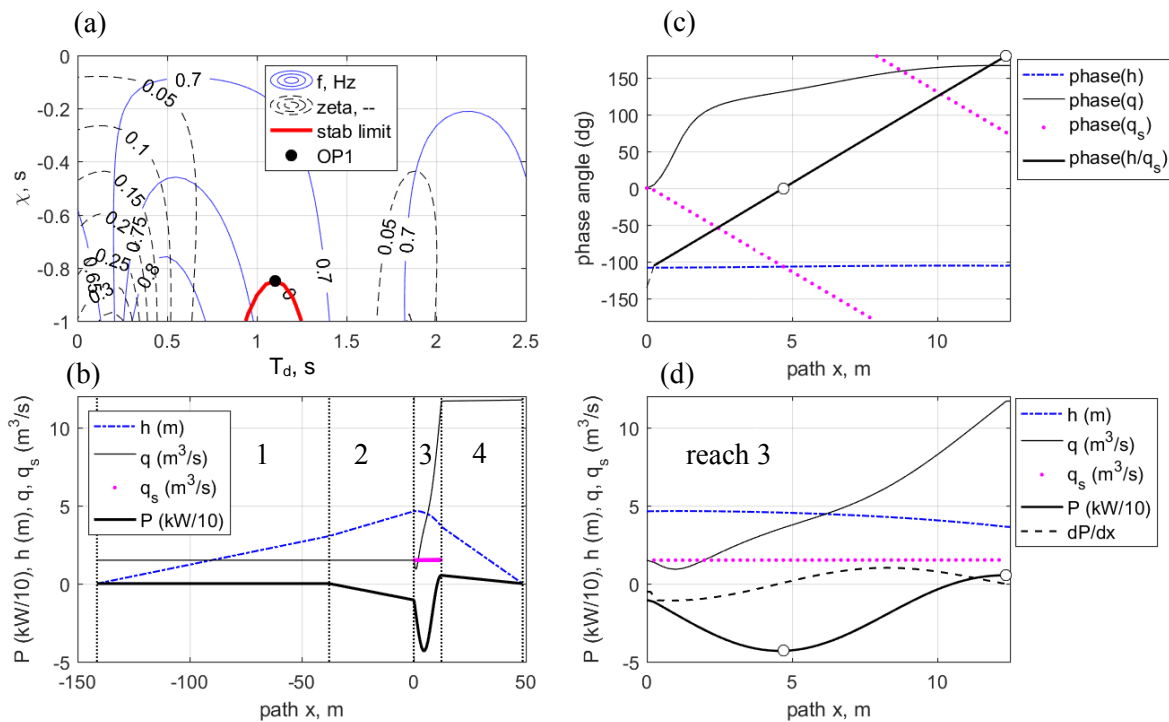


**Figure 5.** (a) Stability diagram for example 1 (b), (d) Amplitudes and (c) Phase angles for point OP1

To explain the energy budget of this oscillation, the mode shape of the head and flow fluctuations for condition OP1 at the stability limit are shown in the diagrams (b) through (d) of Figure 5. In addition to the amplitudes (graphs b, d), the phases are also indicated (graph c). The bold black curve in (b) and (d) indicates the local flux of oscillation power; positive values indicate that power is transported downstream. Parts 2 and 4 of the system upstream and downstream of the draft tube cone consume oscillation power. The phase of the swirl-transporting variable  $q_s$  (pink dots in graph (c)) changes continuously inside the draft tube cone (reach 3 of the system), in the part  $4.7\text{m} < x < 12.4\text{m}$  between the two marked points, its phase against pressure head  $h$  (bold black line in (c)) is between 0 and 180deg. Oscillation energy is supplied from this region to the rest of the system, because due to the negative sign of  $\chi$ , the incremental discharge  $-j\omega \cdot \chi_i \cdot q_{si}$  has a component in phase with the local static pressure  $\rho g h_i$ .

### 3.2. Example 2: Next-higher eigenmode (upper-part-load pulsation)

The next example represents a case of upper-part-load pulsation occurring on a model turbine in a laboratory test rig. The data of the hydraulic system (test rig and model) and the parameters of operation and of the draft tube vortex model are listed in Table 2.

**Table 2.** Example 2, system and operation data

System	Penstock	Casing + runner	DT part 1	DT part 2
Reach	1	2	3	4
L, m	4.0	2.8	0.98	2.4
L/A, 1/m	31.8	29.1	6.7	8.5
R, s/m <sup>2</sup>	0.0	45.2	0.0	0.5

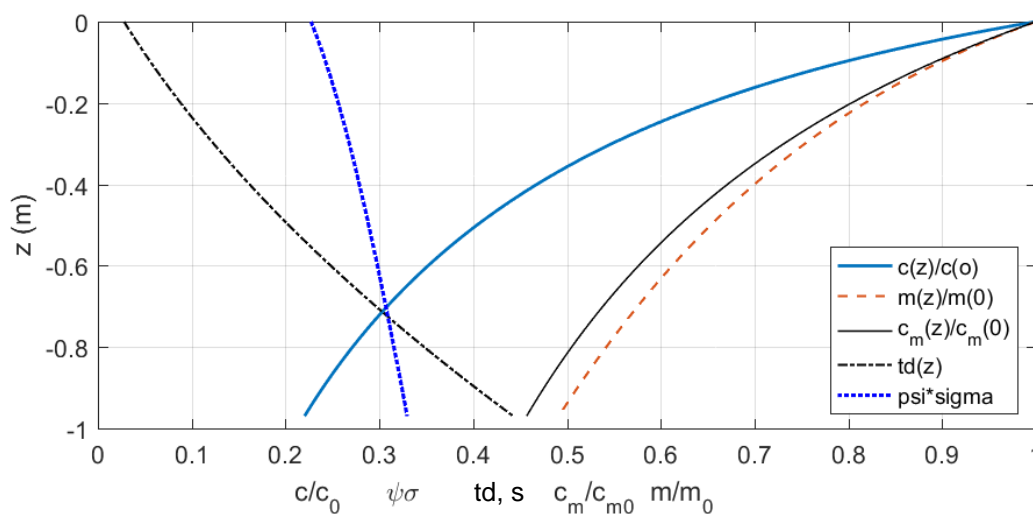
  

Model turbine operation data		
Runner diameter	D, m	0.35
Speed	n, 1/s	15.0
Test head	H, m	10.5
Discharge	Q, m <sup>3</sup> /s	0.36
BEP discharge	Q <sub>opt</sub>	0.48
Specific speed	n <sub>Qopt</sub>	107
Cavitation index	$\psi\sigma$	0.27
Cav. compliance	C, m <sup>2</sup>	6.6e-4
Mass flow gain	$\chi$ , s	0.05

Prototype data		
Runner diameter	D, m	4.90
Speed	n, 1/s	2.0833
Head	H, m	40.0

Unlike the previous example, the axial distribution of the cavitation influence versus path length  $x$  is of high importance for the more complex mode shape of this second eigenmode. The assumption of a uniform distribution as in the previous section would be too far from reality. In [12] the author introduced a method for estimating the distribution of the compliance parameter  $c = \partial C / \partial x$  based on a model test series where the cavitation coefficient  $\sigma$  is varied for a given test condition. The product  $\psi\sigma$  is used here because, unlike  $\sigma$ , it is invariant to changes of  $n_{ED}$  and even  $n_{QE}$ . Figure 6 presents the distribution of compliance  $c$  according to this concept, with the vertical coordinate  $z$  as vertical axis. In the interesting vertical part of the draft tube, the path length is  $x = -z$  (assuming zero at the draft tube intake). The nominal trajectory of swirl travel  $td = (1/Q) \cdot \int dx/A(x)$  is also shown in Figure 6. It may start at  $z=0$  with a non-zero value as discussed in section 4.3. The distributed mass flow gain  $m(x) = \partial\chi/\partial x$  has been estimated from a set of cavity volumes with different  $Q$  based on ref. [12].



**Figure 6.** Distributed parameters of draft tube cone and vortex

The streamwise reduction of the distributed compliance  $c$  and mass flow gain  $m$  shown in Figure 6 is controlled by a local cavitation factor  $\psi\sigma$  which (unlike  $\psi\sigma$  in Table 2) considers the gravity and pressure recovery effect in the draft tube. This effect is modelled by the equations

$$c(z) = c(0) \cdot \exp(bc \cdot (\psi\sigma(z) - \psi\sigma(0))) \quad bc = -14.8 \quad (4)$$

$$m(z) = m(0) \cdot \exp(bm \cdot (\psi\sigma(z) - \psi\sigma(0))) \quad bm = -6.9 \quad (5)$$

where  $c(0)$  and  $m(0)$  are selected such as to fulfil  $\int c \cdot dx = C$  and  $\int m \cdot dx = \chi$ .

The function  $td(x)$  in Figure 6 starts with a finite value. This accounts for the finite meridional distance between the runner blade trailing edges and the onset of the draft tube rope.

With the data of example 2, the time required for a swirl disturbance to travel from the draft tube entry to the end of the cavitation zone ( $x=0.98\text{m}$ ) is

$$T_d = td(L_c) = \int A(x) \cdot dx / Q = 0.42\text{s} \quad (6)$$

The vortex model with these properties is embedded in a system according to Figure 2. The ‘runner’ (reach 2 in Table 2) is an incompressible element composed of inertia  $L/Ag$  and resistance  $R$ . The cavitating section (reach 3) is represented by  $n_s (=100)$  ‘slices’ of identical structure like Figure 1.

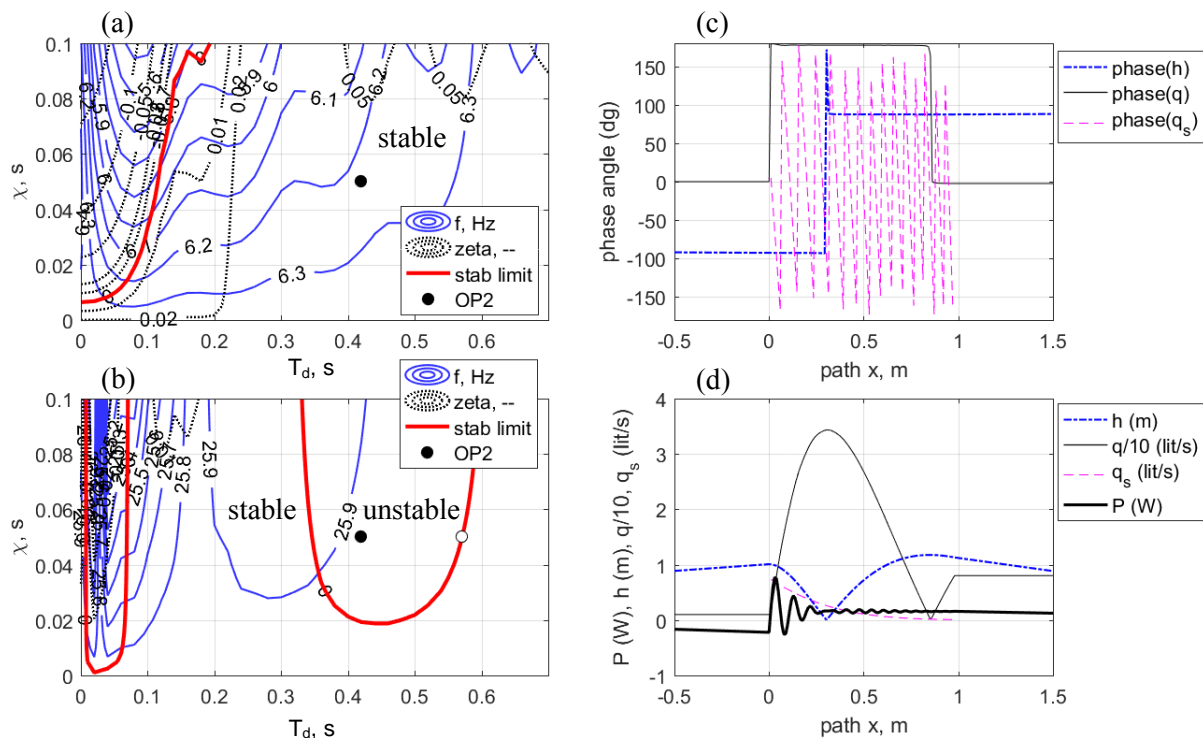


**Figure 7.** Example 2: Stability diagram lowest (a) and second-lowest mode (b), mode shape/power flow (c, d)

The stability diagrams resulting for the two lowest eigenmodes are presented in Figure 7. The lowest eigenmode (a) may be subject to resonance in an ordinary forced partial-load oscillation. This mode is always stable. (Note that, due to the positive sign of  $\chi$ , mode 1 would inevitably become unstable if  $T_d$  were zero.) The next-higher eigenmode (b) is the one occurring in the ‘upper-part-load pulsation’ if the actual combination of  $\chi$  and  $T_d$  happens to be inside the unstable range like the chosen point OP2, with  $\chi=0.05\text{s}$  and  $T_d=0.42\text{s}$ . In this example the upper part load pulsation has a frequency of 25.9 Hz, or 1.72 times the runner frequency.

For a point shifted to the stability limit ( $T_d=0.57s$ ) of this mode, the mode shape and the flow of oscillation energy are shown at the right-hand side of Figure 7. The process is more complex compared to the low-frequency mode described in example 1 because, due to the high frequency, there are many oscillation cycles of the swirl variable  $q_s$  along the cavity. As shown in the diagrams (c) and (d), the axial wavelength of this torsional oscillation is only a few centimeters. One must expect that due to turbulent shear the amplitude of the swirl variation is dropping considerably along the path. This decay is approximated by the following law (compare Figure 1)

$$q_{si+1} = q_{si} \cdot k_i(s) = q_{si} \cdot \exp(-s t_{d_{i+1}}) \cdot \exp(\mu \cdot \text{abs}(s t_{d_{i+1}})) \quad \mu = -0.05 \quad (7)$$

Figure 7 (d) demonstrates very clearly the importance to distinguish between the different oscillation processes superimposed on the vortex. The wall pressure mode has approximately two quarter waves with a single reversal of phase. The oscillation of swirl, due to its low speed, has many cycles; it just supplies oscillation power and does not stand out in any measured signal. The amplitude of flow at draft tube exit is about 6 times higher compared to penstock flow. But compared to both of them, flow amplitude is still much higher at the pressure node inside the draft tube cone.

#### 4. Parameter study

##### 4.1. Variation of Froude number and test head

Maintaining the model and test installation used in section 3.2 and its operation parameters  $n_{ED}$ ,  $Q_{ED}$  and  $\sigma$ , the influence of changing the pressure scale will now be examined. The test head is varied over a wide range, and the two lowest eigenvalues are computed considering the influence of local pressure on the distributed compliance and mass flow gain. The Figure 8 shows some results. Without gravity effects, the cavitation compliance would scale with  $H^{-1}$ , however, for very small test head the lower parts of the vortex become much less compliant. This results in an increase of both relative natural frequencies. The lowest test head (o) would have the same Froude number as a prototype with  $D=4.9m$ ,  $H=40m$ ; in a laboratory test this condition would be spoiled by problems with dissolved gas. According to diagram (b), the unstable condition would only prevail in a range of test heads between 5.1 and 21.5m. Higher and lower head values (including the Froude number of prototype) are stable.

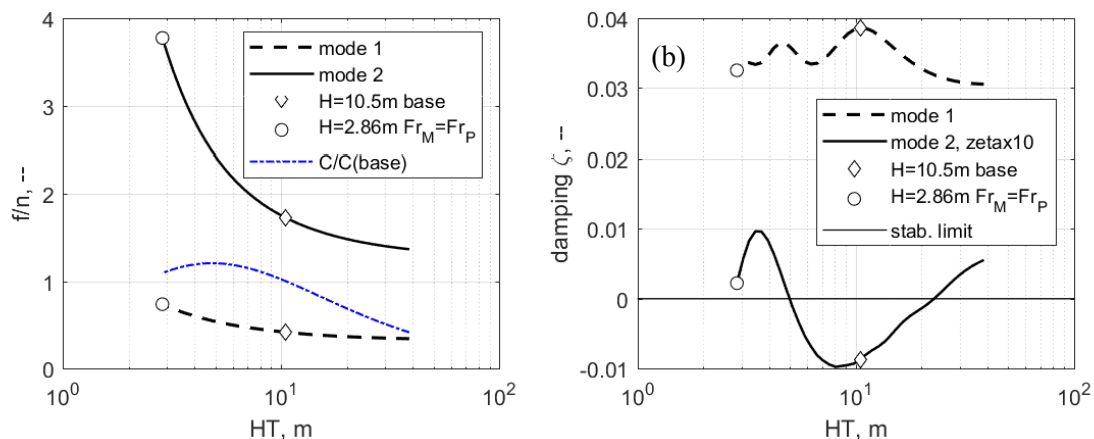
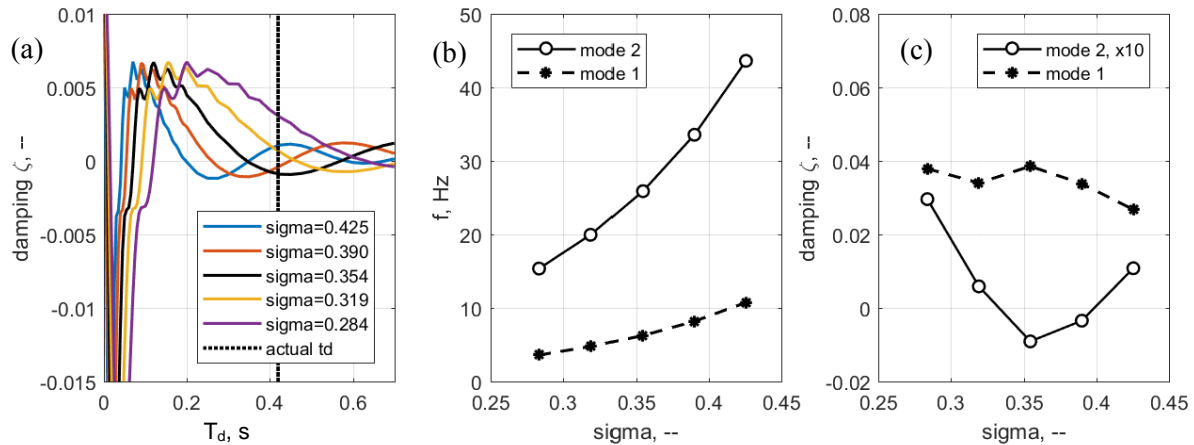


Figure 8. Influence of test head / Froude number

##### 4.2. Variation of cavitation number

Based on the equations (4) and (5), the parameters *compliance* and *mass flow gain* can be transposed to a different draft tube pressure level if the point of operation (test head and discharge) is not changed. For a number of stepwise increased and decreased values of the cavitation number, the first two eigenvalues have been evaluated, considering this shift of  $C$  and  $\chi$ . The Figure 9 shows some results. The two lowest natural frequencies shift in an approximately proportional manner (b). The

lowest mode is always stable (c) but the mode 2 (upper part load pulsation) is unstable in some limited range of  $\sigma$  around the base case  $\sigma=0.354$ . Diagram (a) explains why this is so: positive balance of oscillation power (negative damping) requires the ratio between oscillation period ( $1/f$ ) and wave travel time  $T_d$  to be in a certain range; outside of this range there is no surplus of oscillation power.



**Figure 9.** Influence of draft tube pressure level

#### 4.3. Variation of hub extension

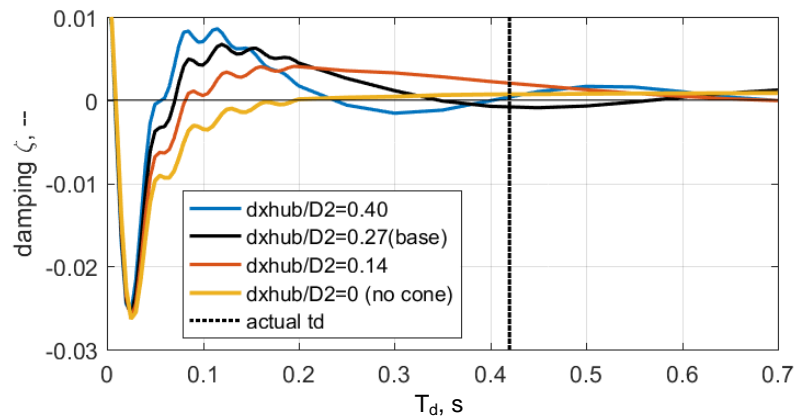
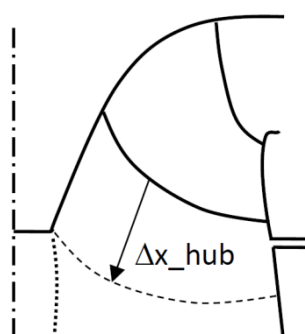


**Figure 10.** Influence of swirl shift due to hub length

The meridional distance between the runner blades and the attachment point of the vortex has a critical influence on the phase of the swirl in the upper draft tube cone. In the 1D model, the shifting of this phase may be approximated by a time delay  $td_0 = \Delta x_{hub} \cdot A/Q$  added to the trajectory  $td(x)$  as shown at the top of Figure 6. This parameter has indeed influence on stability. According to the damping values in Figure 10, the unstable condition in the base case may be removed either by making the runner cone somewhat longer, or by removing it - as observed by Kuznetsov et al [13] in a model test.

#### 4.4. Variation of upstream impedance

A model test context has been chosen for the sample case 2 in section 3.2 because most published information is from model tests; questions about transposability to prototype are obvious. Apart from the influence of the Froude number (section 4.1), the non-similar upstream part of the system should also play a role. The self-excited pulsation corresponds to an eigenmode of the entire hydraulic system, not only the draft tube. Seen from the draft tube, the upstream hydraulic impedance  $Z_{up}$  at the runner exit represents the rest of the system. With some simplification,  $Z_{up}$  has a real part  $R_T \sim H/Q$  contributed by the runner and an imaginary part (inertance) contributed by the penstock.

The influence of upstream inertance may be visualized by comparing results for different length of the upstream piping (including spiral casing). The base case corresponds to  $L_{up}=6m$ . A variation of this parameter may produce a slight variation of the natural frequency as in Figure 11 (a); this could probably correspond with observations reported by Koutnik et al 2008 [7]. Some effect of the runner resistance  $R_T$  on the damping ratio may be expected; at the right-hand side of Figure 11 this parameter is translated to the corresponding value of prototype head, assuming that the speed and runner exit flow remain unchanged. The result illustrates that the excitation mechanism may produce instability only in case of relatively low runner resistance, i.e. high specific speed.

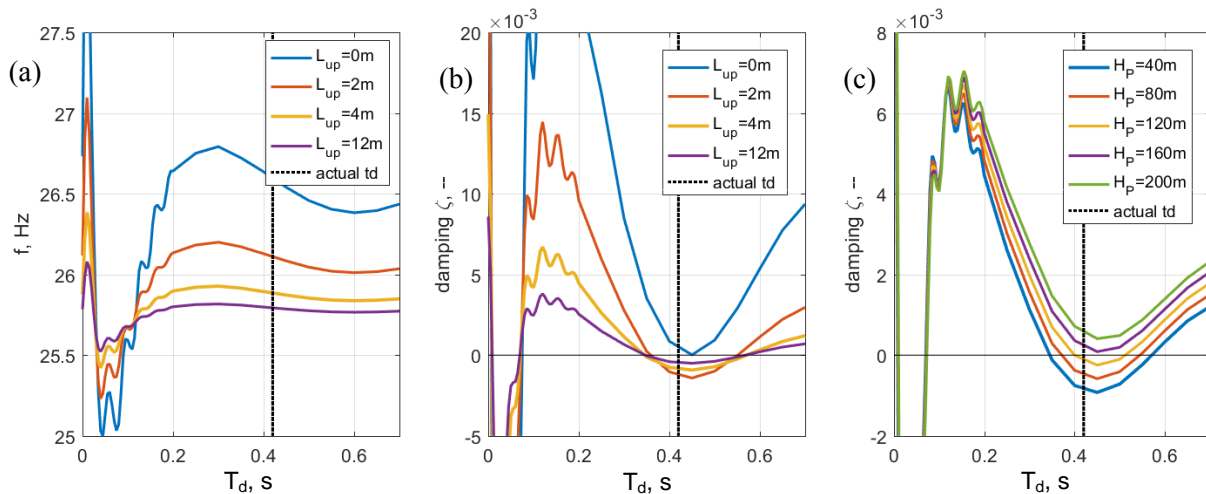


**Figure 11.** Influence of penstock impedance (left, middle) and specific speed (right)

## 5. Conclusion and discussion

The sample calculations in sections 3.2 and 4 demonstrate how the propagation of swirl variations along the cavitating vortex can provoke instability under certain circumstances. The results are in good agreement with the properties commonly ascribed to the upper-part-load oscillation. The examples thus confirm that a synchronous type of hydraulic instability is the cause of this particular phenomenon; this was the goal of the study.

It was not the purpose of this study to promote a method of prediction, let alone pretend such prediction may be relied on given today's state of knowledge. There are mainly two difficulties:

- No reliable prediction of damping effects for this 2-phase flow is available. Parameters in available cavitation models [6] would have to be experimentally validated for this unsteady application. Diffuser effect as well as unsteady damping was neglected here, see Figure 1.
- Proper estimation of distributed parameters. The balance of oscillation power depends on the distribution of compliance and mass flow gain, even if the integral values  $C$  and  $\chi$  are correct. The makeshift assumption of constant cavity length goes into this category.

In addition, the mechanism of swirl propagation and decay has been simplified for the purpose of demonstration. The axial velocity in the real flow is not uniformly distributed, thus the velocity of swirl transport may deviate from the model. The value of exponent  $\mu$  modelling the decay of swirl variation in equation (7) had to be estimated; only its order of magnitude may be correct. Also the helical vortex shape is not represented.

Last but not least, the use of the steady-state turbine impedance for the high frequencies concerned is highly questionable. In ref. [8] it was shown that the finite velocity of swirl transport may also play a role in the vaneless space upstream of the runner. As the relative width of this space increases at high specific speed, this holds in particular for low-head turbines. The actual runner resistance, and hence also the damping ratio, may therefore deviate considerably from the usual steady-state approximation.

### Nomenclature

$A$	Cross-section area [m <sup>2</sup> ]	$n_{QE}$	Specific speed IEC 60193 [-]
$bm, bc$	Coefficient for influence of $\psi\sigma$ [-]	$p$	static pressure [Pa]
$C$	Total cavitation compliance [m <sup>2</sup> ]	$P, P_{osc}$	oscillation power [W]
$c$	Local cavitation compliance [m]	$Q, q$	Discharge [m <sup>3</sup> /s]
$D$	Diameter [m]	$r, R$	Radius, cavity radius [m]
$f$	Frequency [Hz]	$td, T_d$	Swirl transport delay [s]
$g$	Gravity acceleration [m/s <sup>2</sup> ]	$x, z$	Path length, vertical coordinate [m]
$H$	Turbine net head [m]	$V_C$	Volume of cavity [m <sup>3</sup> ]
$h$	Piezometric head [m]	$Z$	hydraulic impedance [s/m <sup>2</sup> ]
$k(s)$	Swirl reduction factor [-]	$\rho$	Fluid Density [kg/m <sup>3</sup> ]
$L_C$	Axial length of cavitation zone [m]	$\sigma$	Local cavitation number [-]
$m$	Mass flow gain per unit length [s/m]	$\omega$	Angular frequency [rad/s]
$n$	Model runner speed [1/s]	$\psi$	Head coefficient [-]
$n_{ED}$	Speed factor IEC 60193 [-]	$\zeta$	Damping ratio [-]

### References

- [1] Dörfler P K, Sick M and Coutu A 2013, *Flow-Induced Pulsation and Vibration in Hydroelectric Machinery*, London: Springer
- [2] Jacob Th, Prenat J-E 1990, Generation of hydro-acoustic disturbances by a Francis turbine model and dynamic behavior analysis, *IAHR 15th Symp. Hydr. Machinery and Cavitation*
- [3] Dörfler P K 1993, Observation of pressure pulsations at high partial load on a Francis model turbine with high specific speed, IAHR WG1 meetg 1993, and: *Hydropower & Dams*, Jan. 1994
- [4] Arpe J A 2003, *Analysis of the wall pressure field in an elbow-type Francis draft tube* (in French), PhD thesis no. 2779, EPFL Lausanne (CH)
- [5] Koutnik J and Pulpitel L 1996, Modelling of the Francis turbine full-load surge, *Modelling, Testing & Monitoring for Hydro Powerplants – II* ( Lausanne, Switzerland)
- [6] Zwart P J, Gerber A G and Belamri T 2004, A two-phase flow model for predicting cavitation dynamics *Proc. of the 5th International Conf. on Multiphase Flow*, Yokohama, Japan
- [7] Koutnik J, Faigle P, Moser W 2008, Pressure fluctuations in Francis turbines – theoretical prediction and impact on turbine, *Proc. IAHR 24th Symp. Hydr. Machinery and Systems*
- [8] Dörfler P K 1982, *System oscillations excited by the Francis turbine's part load vortex core: mathematical modeling and experimental verification*, PhD thesis (in German) TU Wien (AT), English translation (2013) on researchgate.net
- [9] Dörfler P K 2018, Analysis of the Francis turbine upper-part-load pulsation, Part I – Experimental results vs. hydro-acoustic model, *29th IAHR Symp. Hydr. Machinery and Systems*
- [10] Brennen C E and Acosta A J 1976, The Dynamic Transfer Function of a Cavitating Inducer, *ASME J. Fluids Eng.*
- [11] Dörfler P K, Keller M and Braun O 2010, Full-load surge mechanism identified by unsteady 2-phase CFD, *Proc. IAHR 25th Symp. Hydr Machinery and Systems* (Timisoara, 2010)
- [12] Dörfler P K 2017, Cavitation Compliance in 1D Part-Load Vortex Models, *Intl. J. Fluid Machinery and Systems*, Vol. 10, No. 3
- [13] Kuznetsov I, Zakharov A, Arm V and Akulaev R 2014, Model and prototype investigations of upper partial load unsteady phenomena on the Francis turbine designed for head up to 120 m, *Proc. IAHR Section Hydr Machinery and Cavitation 27th Symp.* (Montreal, 2014)